Size controllable synthesis of cobalt vanadate nanostructures with enhanced photocatalytic activity for the degradation of organic dyes

Maryam Ghiyasiyan-Arani [a], Maryam Masjedi-Arani [b], Masoud salavati-Niasari [a*]

[a] Institute of Nano Science and Nano Technology, University of Kashan, Kashan, P. O. Box.87317-51167, I. R. Iran.

[b] Young Researchers and Elite Club, Arak Branch, Islamic Azad University, Arak, Iran.

** Corresponding author. Tel.: +98 315 5912383; Fax: +98 315 5913201; E-mail address: salavati@kashanu.ac.ir*

Abstract Different types of cobalt vanadate nanostructures such as $Co_3V_2O_8$, $Co_2V_2O_7$ and CoV_2O_6 have been successfully prepared via a simple solid-state method. For the first time, cobalt vanadate nanostructures were synthesized via Schiff-base ligand and vanadyl sulfate as a capping agent and vanadium source, respectively. The effect of a Schiff-base ligand (N,N-Bis (salicylaldehyde) ethylenediamine = H_2salen) as a capping agent, molar ratio of Co: H_2salen and Co:V on type of products, morphology and size of cobalt vanadate nanoparticles was investigated to reach optimum condition. The as-prepared nanostructures were characterized by X-ray diffraction (XRD), scanning electron microscopy (SEM), transmittance electron microscopy (TEM), Fourier transform infrared (FT-IR) spectra, energy dispersive X-ray microanalysis (EDX) and ultraviolet–visible (UV–Vis) spectroscopy. This work is the first study on photocatalytic activity of cobalt vanadate nanostructures in different conditions. The influence of different parameters such as type of cobalt vanadate nanostructures, type of dye, size of particles and nanostructures dosage as a catalyst on photocatalytic activity of samples were studied.

Keywords: Nanostructure; Solid-state method; Electron microscopy; Photocatalytic activity.

1. Introduction:

Today, environmental pollutions and energy shortages have become two serious crisis for future of the world. So using technology based on renewable energy sources to clean up pollution is an essential task. Semiconductor

photocatalyst is one of the most common and useful technologies to reduce or destruction of pollution because it illustrates simple condition to utilize natural or artificial irradiation that is available everywhere. Moreover, material in nano scale show unique properties compared to what they show in micro scale. Catalytic behavior is not only strongly materials-dependent but also extremely size-dependent. Henglein showed that a nanomaterial can exhibit very different behaviors compared to its bulk self [1]. For this purpose, nanomaterials use as photocatalyst due to increasing surface to volume ratio which raise surface energy associated with particles. The various types of photocatalysts are available that most famous of them can be noted TiO_2 [2, 3] But researches continue to replace or improve the properties of the photocatalyst materials. However, wide band gap (3.2 eV) of TiO_2 caused researchers to reduce band gap of photocatalyst material which exposed to visible light for destruction of organic dyes. A series of compounds with low band gap are vanadates such as $BiVO_4$ [4, 5], $FeVO_4$ [6, 7], $AgVO_3$ [8, 9], Ag_3VO_4 [10, 11], $Cu_3V_3O_8$ [12, 13] and $Zn_3V_2O_8$ [14, 15]. Cobalt vanadate, as one of the most important family of vanadate materials, have suitable band gap for the destruction of pollutants. There are numerous classes of cobalt vanadates such as $Co_3V_2O_8$ [16, 17], $Co_2V_2O_7$ [18, 19] and CoV_2O_6 [20, 21]. Many inquiries have been carried out on the synthesis routes of cobalt vanadates including precipitation [22], solid-state [23], sol-gel [24], hydrothermal [25, 26] and electrospinning [27]. These category of vanadates have wide applications in the fields of Sensing electrode [24], pseudocapacitive electrode material or electrochemical capacitive properties [28], electrocatalytic oxygen evolution reaction [27], electrodes for asymmetric supercapacitors [29], lithium ion batteries [30] and water oxidation [31]. Herein, for the first time three types of cobalt vanadate nanostructures were synthesized by simple, green, low-cost, free solvent and reproducible solid-state method in presence of Schiff base ligand as a capping agent. Schiff base ligand have a functional head group (containing hard atoms (N, O)) and one or more hydrocarbon tails, and both elements play a role in the control of nucleation and growth. It has been demonstrated that these kind of organic agents have an effective role on controlling size, shape and properties of final products [32-34]. Effect of molar ratio of Co: H_2salen and Co:V on type of products, morphology and size was investigated. Finally, photocatalytic activity of cobalt vanadate nanostructures were studied in different conditions for the first time. The ability to destroy organic dyes methylene blue, methyl violet, eosin Y and erythrosine under UV and Vis irradiations were

measured using photocatalysis test. The influence of different parameters such as type of cobalt vanadate nanostructures, type of dye, size of particles and nanostructures dosage as a catalyst on photocatalytic activity of samples were scrutinized. The results of these tests show $Co_3V_2O_8$ can utilize as photocatalyst material along with other photocatalyst product to increase efficiency.

2. Experimental

2.1. Materials

All the chemicals reagents for the synthesis of cobalt vanadate nanostructures such as Co $(CH_3COO)_2.4H_2O$, $VOSO_4.5H_2O$, salicylaldehyde and 1,2-ethylenediamine were of analytical grade and were used as received without further purification. N,N-bis(salicylidene)-ethylene-1,2-diamine, [H_2salen], precursor was synthesized according to previous procedure [35, 36].

2.2. Characterization

X-ray diffraction (XRD) patterns were recorded by a Philips-X'pertpro, X-ray diffractometer using Ni-filtered Cu Ka radiation. Fourier transform infrared (FT-IR) spectra were detected by means of Nicolet Magna-550 spectrometer in KBr pellets. Scanning electron microscopy (SEM) images were obtained through LEO-1455VP equipped with an energy dispersive Xray spectroscopy. GC-2550TG (Teif Gostar Faraz Company, Iran) were used for all chemical analyses. The EDX analysis with 20 kV accelerated voltage was done. Transmission electron microscopy (TEM) image was achieved via a Philips EM208 transmission electron microscope with an accelerating voltage of 200 kV.

2.3. Synthesis of cobalt vanadate nanostructures

The different types of cobalt vanadate nanostructures were prepared using a simple solid-state method. $Co(CH_3COO)_2.4H_2O$, $VOSO_4.5H_2O$ and H_2salen Schiff-base were weighted and mixed. Each mixture of the starting powders was milled and mixed in a ball mill for 1 h using zirconia grinding media. The powder product was calcined at different temperatures. The different preparation conditions for synthesis of cobalt vanadate nanostructures have been illustrated in Table 1. To study the effect of H_2salen Schiff-base on the morphology and size of the products, an experiment as blank test was carried out without Schiff-base. Moreover, the effect of

molar ratio of Co: H_2salen and Co:V on type of products, morphology and size were investigated. In Scheme 1, schematic diagram of formation of cobalt vanadate nanostructures is depicted.

2.4. Photocatalytic measurements

The photocatalytic activity of cobalt vanadate nanoparticles was tested by using different dyes solution. The degradation reaction was performed in a quartz photocatalytic reactor. The photocatalytic degradation was carried out with 0.0005 g of dye solution containing 0.05 g of nanostructures. This mixture was aerated for 30 min to reach adsorption equilibrium. Then, the mixture was placed inside the photoreactor in which the vessel was 40 cm away from the UV and visible source. The quartz vessel and light sources were placed inside a black box equipped with a fan to prevent UV leakage. The experiments were executed at room temperature. The effect of different cobalt vanadate products, cationic or anionic dyes and size of product on photocatalytic properties was deliberated. Aliquots of the mixture were taken at periodic intervals during the irradiation, and after centrifugation they were analyzed with the UV–vis spectrometer.

3. Results and discussion

3.1. X-ray diffraction patterns

In order to confirm the crystal phase and purity of the products, XRD analyses were applied. XRD patterns of the products synthesized at different calcination temperatures and molar ratios of Co:V are shown in Fig. 1. Fig. 1a shows XRD pattern of product obtained at 500 °C (sample No. 2). According to this pattern, temperature of 500 °C is not sufficient for synthesis of cobalt vanadate nanostructures. Fig. 1b-d show XRD patterns of samples prepared at different Co:V molar ratios of 3:2 (sample No. 3), 1:2 (sample No. 6) and 1:1 (sample No. 7), respectively. In Fig. 1b with increasing calcination temperature to 600 °C, most of the reflection peaks can be attributed to the orthorhombic phase $Co_3V_2O_8$ (JCPDS card No. 74-1486). The as-synthesized product at molar ratio of Co:V = 1:2 (sample No. 6) consists ofCoV_2O_6nanocrystals with two crystal system (JCPDS card No. 77-1174 and 45-1052). Fig. 1d shows as-prepared sample at molar ratio of Co:V = 1:1 (sample No. 7) including Monoclinic phase $Co_2V_2O_7$ (JCPDS card No. 70-1189). The details of Crystal parameters of cobalt vanadate nanostructures were presented in Table. 2. The crystallite diameter (Dc) of different cobalt vanadate nanostructures obtained using the Scherrer equation [37, 38]:

$$D = K\lambda/\beta\cos\theta \quad (1)$$

where β is the breadth of the observed diffraction line at its half intensity maximum, K is the so-called shape factor which usually takes a value of about 0.9, and λ is the wavelength of X-ray source used in XRD. Calculated crystalline domain sizes have been shown in Table. 1.

3.2. SEM and TEM images

To examine the role of the H_2salen Schiff-base as a capping agent on the morphology and size of the products, cobalt vanadate nanostructures were synthesized with different molar ratios of Co: H_2salen via simple solid-state method. Fig. 2a-l exhibit SEM images of cobalt vanadate samples prepared with different molar ratios of Co: H_2salen. SEM images of the product obtained from the blank test without H_2salen Schiff-base in different scales are shown in Fig. 2a-c. According to the Fig. 2a-c, it can be seen that the product have very irregular morphology and large size. Fig. 2d-l display SEM images of as-prepared products with molar ratios of Co: H_2salen = 1:0.5, 1:1 and 1:2 (sample No. 3-5), respectively. It is observed that with increasing Schiff-base concentration, an increase in particle size occurs. This trend is possibly due to the presence of extra H_2salen Schiff-base. The optimum amount of H_2salen could readily adsorb on the crystal facets of cobalt vanadate without any repulsion or attraction by its similar neighboring molecules. Increasing the concentration of H_2salen Schiff-base will enhance the percentage of free H_2salen Schiff-base which could easily form hydrogen bond with themselves and finally synthesized agglomerated products as shown in Scheme. 2. These results indicate that molar ratio of Co: H_2salen = 1:0.5 is very favorable to produce fine and uniform $Co_3V_2O_8$ nanoparticles. The particle sizes of cobalt vanadate products were represented in Table. 1.

To inspect the effect of the H_2salen Schiff-base as a capping agent on the size distribution of the products, cobalt vanadate nanostructures were studied with histograms of the particle diameters for different molar ratios of Co: H_2salen. Typical histograms of the particle diameters for the samples Nos. 3-5 are perceived in Fig. 3a-c, respectively. By comparing the particle size distribution of the products, it is found that cobalt vanadate prepared with molar ratio of Co: H_2salen = 1:0.5 have smaller particle size distribution (20–70 nm). Also, cobalt vanadate prepared with molar ratio of Co: H_2salen = 1:2 have the largest particle size distribution.

Fig. 4a-f show SEM images of CoV_2O_6 and $Co_2V_2O_7$ nanoparticles prepared in different molar ratios of Co:V in presence of H_2salen Schiff-base, respectively. As shown in Fig. 4, CoV_2O_6 and $Co_2V_2O_7$ nanostructures have more agglomeration from $Co_3V_2O_8$ nanoparticles.

The exact morphology and size of $Co_3V_2O_8$ nanostructures prepared in presence of the H_2salen Schiff-base was illustrated by TEM images. Fig. 5 show the TEM images of sample No. 3 which contains homogenous spherical nanoparticles with the size of around 10-15 nm. As shown in Figure 5 in HRTEM images, the distance between the two adjacent planes, d, is measured to be 0.218 nm.

3.3. EDX and FT-IR analysis

To explore the chemical interactions and bonding structures, Fig. 6a-c have been dedicated to the FT-IR spectra of the cobalt vanadate nanoparticles (sample No. 3, 6 and 7). The absorption from 3000 to 3600 cm^{-1} can be assigned to the stretching vibration of the hydrogen bonded OH groups of the adsorbed water. The absorption around 1620 cm^{-1} is due to the bending vibration of water molecules. In addition, the adsorption peaks located around 1135 cm^{-1} could be related to the absorptions of CO_2 molecules from the atmosphere in Fig. 6. The band around 420 cm^{-1} in the FT-IR spectrum belongs to the stretching mode of the inorganic Co-O. According to previous reports, the vibration bands in the range of 930–650 cm^{-1} are attributed to tetrahedral VO_4. Fig. 6d shows FT-IR spectrum of sample No. 3 before calcination. The (C=N) stretching vibration band at 1644 cm^{-1} , The ring skeletal vibrations (C=C) of Schiff-base ligand in the region of 1447-1554 cm^{-1} and phenolic C–O stretching vibration band at 1291 cm^{-1} indicates the presence of H_2Salen Schiff-base ligand before calcination (Fig. 6d) which completely disappear after calcination at 600 ˚C (Fig. 6a). From the FT-IR results, it can be concluded that an amount of ligand is attached to the surface of nanoparticles which can have an effective role in preventing nanoparticles agglomeration.

The purity and chemical composition of the cobalt vanadate nanostructures was also confirmed by energy dispersive X-ray spectroscopy. EDX analysis of CoV_2O_6, $Co_2V_2O_7$ and $Co_3V_2O_8$ nanoparticles are revealed in Fig. 7a-c. The lines of Co, V and O are obviously observed. The atomic percentages of elements have good agreement with type of cobalt vanadate nanostructures.

3.4. Optical properties

Investigating the energy structures and optical properties of semiconductor cobalt vanadate nanostructures, The UV–Vis diffuse absorption spectrum was studied. The absorption spectra of $Co_3V_2O_8$, $Co_2V_2O_7$ and CoV_2O_6 nanoparticles are shown in Fig. 8. It is apparent that the CoV_2O_6 nanoparticles absorption edge was shifted to the higher-energy region than $Co_3V_2O_8$ and $Co_2V_2O_7$ nanoparticles. The fundamental absorption edge in most semiconductors follows the exponential law [28]. Using the absorption data, the band gap was estimated by Tauc's relationship:

$$\alpha = \frac{\alpha_0(h\upsilon - E_g)^n}{h\upsilon} \quad (2)$$

where α is absorption coefficient, hν is the photon energy, α_0 and h are the constants, E_g is the optical band gap of the material, and n depends on the type of electronic transition and can be any value between 1/2 and 3 [39]. The energy gaps of the samples have been determined by extrapolating the linear portion of the plots of $(\alpha h\nu)^{1/2}$ against hν to the energy axis. The Eg values are calculated 2.71, 2.85 and 3.19 eV for the $Co_2V_2O_7$, $Co_3V_2O_8$ and CoV_2O_6 nanoparticles, respectively.

3.5. The photocatalytic activity of nanostructures

The influence of different parameters such as type of cobalt vanadate nanostructures, type of dye, size of particles and nanostructures dosage as a catalyst on photocatalytic activity of samples were investigated by monitoring the degradation of organic dyes as water pollutants in an aqueous solution. 3.5.1. *Effect of type of cobalt vanadate*

As shown in Fig 9a, the photocatalytic activity improves in the order of $Co_2V_2O_7$, CoV_2O_6 and $Co_3V_2O_8$ under UV irradiation. The $Co_2V_2O_7$ nanoparticle shows the poorest photodegradation efficiency, and only 23% of methylene blue solution was degraded after 120 min irradiation. At the same photodegradation condition, the degradation efficiency was 39% for CoV_2O_6. The $Co_3V_2O_8$ nanostructures show better photocatalytic activity, and the corresponding degradation efficiency reaches 87%. As a result, in variety of cobalt vanadate compounds, the best performance was achieved for destruction of MB in presence of $Co_3V_2O_8$.

3.5.2. *Effect of Dye*

Fig. 9b shows the effect of different anionic (eosin Y and Erythrosine) and cationic (methylene blue and Methyl violet) dyes on photocatalytic activity of optimized $Co_3V_2O_8$ nanostructure samples. It is obvious in Fig. 9b that

the photocatalytic activity of cationic dyes is better than anionic dyes. The photodegradation efficiency of Erythrosine, eosin Y, methylene blue and Methyl violet are 29, 39, 87 and 88%, correspondingly. It was found that in photocatalytic degradation, the adsorption level on $Co_3V_2O_8$ is higher for dyes with a positive charge (cationic) than for those with a negative charge (anionic). This fact can be explained in relation to the surface structure of $Co_3V_2O_8$ nanostructures. On the surface of $Co_3V_2O_8$ nanocrystal, oxygen atoms with a high electron density are present. Thus, $Co_3V_2O_8$ have negative charge and therefore adsorb the cationic molecules [40, 41]. The highest values of photocatalytic degradation is for cationic methyl violet dye.

3.5.3. *Effect of size of catalyst*

The photocatalytic activity of nano and bulk structures of $Co_3V_2O_8$ in presence of H_2salen Schiff-base (sample No. 3) and without H_2salen Schiff-base (sample No. 1) were compared under UV light irradiation. The obtained results are shown in Fig. 9c. On the basis of Fig. 9c, the photocatalytic activity of $Co_3V_2O_8$ nanostructures prepared in presence of H_2salen Schiff-base is evidently higher than bulk structures. According to photocatalytic calculations, the MB degradation was about 87 % by $Co_3V_2O_8$ nanostructures and 25 % by $Co_3V_2O_8$ bulk structures after 120 min irradiation of UV light. By decreasing particle size of semiconductors, the surface area to volume ratio and finally available surface active sites and interfacial charge-carrier transfer rates increased and thus leading to higher catalytic activities.

3.5.4. *Effect of catalyst loading*

The effect of $Co_3V_2O_8$ nanostructures dosage on the methyl violet degradation is unveiled in Fig. 9d. By increasing catalyst dosage, the MV degradation is increased. The results indicate that the percentage degradation of MV under UV irradiation increased from 81% to 89% with increasing dosage of nanocatalyst from 0.025 to 0.075 g. photocatalytic activity of cobalt vanadate nanostructures with 0.075 g dosage in the initial stage (0-60 min) is slower than two other dosages. From the photocatalytic activity results, it can be concluded that slower activity may be due to increasing of catalyst amount, opacity of solution and decreasing of absorption of UV irradiations. Also, due to similarity of final degradation percentage for 0.075 and 0.05 g of nanostructure catalyst and slower photocatalytic activity of 0.075 g loading in the initial stage (0-60 min), the optimum catalyst loading is 0.05 g.

3.5.5. Effect of type of irradiation light

Finally, the photocatalytic activity of $Co_3V_2O_8$ nanostructures under UV and visible light irradiation were compared. The obtained results are shown in Fig. 9e. $Co_3V_2O_8$ nanostructures is irradiated with visible light have a relatively good percentage of destruction (70%) for MV as a cationic dye. The MV degradation under UV light irradiation is more than visible light irradiation according Fig. 9e. The chemical formulas of different cationic and anionic dyes as a water pollutant are observed in Fig. 9f. The degradation mechanism of dye for $Co_3V_2O_8$ nanostructures is shown in Scheme. 3.

3.5.6. The stability of cobalt vanadate catalyst

The used cobalt vanadate nanostructures in this work are stable after photocatalytic activity. XRD pattern and FT-IR spectrum of $Co_3V_2O_8$ nanoparticles after photocatalytic activity are shown in Fig. 10a and b, respectively. By comparing of XRD patterns of $Co_3V_2O_8$ nanoparticles before and after photocatalytic activity (Fig. 1b and 10a), it is clear that $Co_3V_2O_8$ photocatalyst is stable. Also, FT-IR spectra of $Co_3V_2O_8$ nanoparticles before and after photocatalytic activity (Fig. 6a and 10b) are same.

3.5.7. Mechanism of photocatalytic degradation

Mechanism of methyl violet dye photocatalytic degradation is shown as follows. When the methyl violet dye was excited by the light irradiation, the electrons from the MV were transferred to the $Co_3V_2O_8$ nanoparticles conduction band. Those electrons were borrowed by the oxygen species present in the water, which were responsible for the production of reactive oxygen radicals. Also the electron–hole pair formed due to excitation of $Co_3V_2O_8$ nanoparticles using UV irradiation provides necessary conditions for the formation of reactive oxygen species leads to the degradation of organic contents found in the aqueous medium. The following equations explain about the various reaction sequences of photo catalytic degradation [42].

$MV + h\nu \rightarrow MV^{*}$

$MV^{*} + Co_3V_2O_8 \rightarrow Co_3V_2O_8^{-1} + MV^{+1}$

$Co_3V_2O_8^{-1} + O_2 \rightarrow Co_3V_2O_8 + O_2^{-1}$

$Co_3V_2O_8 + h\nu \rightarrow Co_3V_2O_8\ (h^{+} + e^{-})$

$h^{+} + H_2O \rightarrow OH + H^{+}$

$H^+ + O_2^- \rightarrow HO_2$

$2\ HO_2 \rightarrow H_2O_2 + O_2$

$H_2O_2 + O_2^- \rightarrow OH + OH^- + O_2$

$H_2O_2 + e^- \rightarrow OH + OH^-$

$MV + ROS \rightarrow$ degraded MV ($CO_2 + H_2O$)

4. Conclusions

Different types of cobalt vanadate nanostructures were prepared via simple solid-state method in presence of H_2salen Schiff base ligand as a novel capping agent. Using vanadyl sulfate as a vanadium source was reported, for the first time. The effect of various parameters including molar ratios of Co: H_2salen and Co:V on type of products, morphology and size of cobalt vanadate nanoparticles was investigated to reach optimum condition. It was well known that using H_2salen Schiff base could prevent the particles from agglomeration. The smallest size of particle is achieved when ratio of Co: H_2salen = 1:0.5 was used. To the best of our knowledge, this project is the first study of photocatalytic activity of cobalt vanadate nanostructures. Moreover, The influence of different parameters such as type of cobalt vanadate nanostructures, type of dye, size of particles and nanostructures dosage as a catalyst on photocatalytic activity of samples were investigated. By comparing three types of cobalt vanadate $Co_3V_2O_8$, $Co_2V_2O_7$ and CoV_2O_6, it was observed that $Co_3V_2O_8$ nanostructures can be used as an interesting candidate for photocatalytic applications under UV and visible irradiation for removal of cationic dyes.

Acknowledgments

Authors are grateful to the council of Iran National Science Foundation and University of Kashan for supporting this work by Grant No (159271/555).

References

[1] A. Henglein, Mechanism of reactions on colloidal microelectrodes and size quantization effects

Top. Curr. Chem. 143 (1988) 113–180.

[2] O. Elbanna, P. Zhang, M. Fujitsuka, T. Majima, Facile preparation of nitrogen and fluorine codoped TiO_2 mesocrystal with visible light photocatalytic activity, Appl. Catal. B: Environ. (2016) doi:10.1016/j.apcatb.2016.03.053.

[3] Y. Cao, X. Li, Z. Bian, A. Fuhr, D. Zhang, J. Zhu, Highly photocatalytic activity of brookite/rutile TiO 2 nanocrystals with semi-embedded structure, Appl. Catal. B: Environ 180 (2016) 551-558.

[4] X. Gao, Z. Wang, X. Zhai, F. Fu, W. Li, The synthesize of lanthanide doped BiVO 4 and its enhanced photocatalytic activity, J. Mol. Liq. 211 (2015) 25-30.

[5] Y. Geng, P. Zhang, N. Li, Z. Sun, Synthesis of Co doped BiVO 4 with enhanced visible-light photocatalytic activities, J. Alloys Compd. 651 (2015) 744-748.

[6] B. Ozturk, G.S.P. Soylu, Synthesis of surfactant-assisted FeVO 4 nanostructure: Characterization and photocatalytic degradation of phenol, J. Mol. Catal. A: Chem. 398 (2015) 65-71.

[7] J. Deng, J. Jiang, Y. Zhang, X. Lin, C. Du, Y. Xiong, $FeVO_4$ as a highly active heterogeneous Fenton-like catalyst towards the degradation of Orange II, Appl. Catal. B: Environ. 84 (2008) 468-473.

[8] V. Sivakumar, R. Suresh, K. Giribabu, V. Narayanan, $AgVO_3$ nanorods: Synthesis, characterization and visible light photocatalytic activity, Solid-State Sci. 39 (2015) 34-39.

[9] T.A. Vu, C.D. Dao, T.T. Hoang, P.T. Dang, H.T. Tran, K.T. Nguyen, G.H. Le, T.V. Nguyen, G.D. Lee, Synthesis of novel silver vanadates with high photocatalytic and antibacterial activities, Mater. Lett. 123 (2014) 176-180.

[10] X. Hu, C. Hu, Preparation and visible-light photocatalytic activity of Ag_3VO_4 powders, J. Solid State Chem. 180 (2007) 725-732.

[11] H. Xu, H. Li, L. Xu, C. Wu, G. Sun, Y. Xu, J. Chu, Enhanced photocatalytic activity of Ag3VO4 loaded with rare-earth elements under visible-light irradiation, Ind. Eng. Chem. Res. 48 (2009) 10771-10778.

[12] M. Ghiyasiyan-Arani, M. Masjedi-Arani, M. Salavati-Niasari, Novel Schiff base ligand-assisted in-situ synthesis of $Cu_3V_2O_8$ nanoparticles via a simple precipitation approach, J. Mol. Liq. 216 (2016) 59-66.

[13] M. Ghiyasiyan-Arani, M. Masjedi-Arani, M. Salavati-Niasari, Facile synthesis, characterization and optical properties of copper vanadate nanostructures for enhanced photocatalytic activity, J. Mater. Sci: Mater. Electron. (2016) 1-8.

[14] F. Mazloom, M. Masjedi-Arani, M. Ghiyasiyan-Arani, M. Salavati-Niasari, Novel sodium dodecyl sulfate-assisted synthesis of $Zn_3V_2O_8$ nanostructures via a simple route J. Mol. Liq.214 (2016) 46-53.

[15] F. Mazloom, M. Masjedi-Arani, M. Salavati-Niasari, Novel size-controlled fabrication of pure $Zn_3V_2O_8$ nanostructures via a simple precipitation approach, J. Mater. Sci: Mater. Electron. 27 (2016) 1-9.

[16] M. Xiao, D. Yang, Y. Yan, Y. Tian, M. Zhou, M. Hao, R. Cheng, Y. Miao, Nanoplates and Nanospheres of $Co_3(VO_4)_2$ as Noble Metal-free Electrocatalysts for Oxygen Evolution, Electrochim. Acta. 180 (2015) 260-267.

[17] M. Xing, L.-B. Kong, M.-C. Liu, L.-Y. Liu, L. Kang, Y.-C., Cobalt vanadate as highly active, stable, noble metal-free oxygen evolution electrocatalyst, J. Mater. Chem A. 2 (2014) 18435-18443.

[18] Y. Luo, X. Xu, Y. Zhang, C.-Y. Chen, L. Zhou, M. Yan, Q. Wei, X. Tian, L. Mai, Graphene oxide templated growth and superior lithium storage performance of novel hierarchical $Co_2V_2O_7$ nanosheets, ACS Appl. Mater. Interfaces. 8 (2016) 2812-2818.

[19] H.A. Almukhlifi, R.C. Burns, Oxidative dehydrogenation of isobutane to isobutene by pyrovanadates, $M_2V_2O_7$, where M (II)= Mn, Co, Ni, Cu and Zn, and Co_2VO_4 and ZnV_2O_4: The effect of gold nanoparticles, J. Mol. Catal. A: Chem. 408 (2015) 26-40.

[20] C. Mondal, A.K. Sasmal, S. Yusuf, M. Mukadam, J. Pal, M. Ganguly, T. Pal, Modified hydrothermal reaction (MHT) for CoV_2O_6 $4H_2O$ nanowire formation and the transformation to CoV_2O_6 $2H_2O$ single-crystals for antiferromagnetic ordering and spin-flop, RSC Adv. 4 (2014) 56977-56983.

[21] Y. Tang, J. Zhou, J. Liu, L. Liu, S. Liang, Facile Synthesis of Cobalt Vanadium Oxides and Their Applications in Lithium Batteries, Int. J. Electrochem. Sci. 8 (2013) 1138-1145.

[22] M.-C. Liu, L.-B. Kong, L. Kang, X. Li, F.C. Walsh, M. Xing, C. Lu, X.-J. Ma, Y.-C. Luo, Synthesis and characterization of $M_3V_2O_8$ (M= Ni or Co) based nanostructures: a new family of high performance pseudocapacitive materials, J. Mater. Chem A. 2 (2014) 4919-4926.

[23] Z. He, T. Taniyama, M. Itoh, Y. Ueda, Flux growth and magnetic anomalies of $Co_3V_2O_8$ crystals, Cryst. Growth Des. 7 (2007) 1055-1057.

[24] F. Liu, Y. Guan, M. Dai, H. Zhang, Y. Guan, R. Sun, X. Liang, P. Sun, F. Liu, G. Lu, High performance mixed-potential type NO_2 sensors based on three-dimensional TPB and $Co_3V_2O_8$ sensing electrode, Sens. Actuators B: Chem. 216 (2015) 121-127.

[25] G. Yang, H. Cui, G. Yang, C. Wang, Self-assembly of $Co_3V_2O_8$ multilayered nanosheets: controllable synthesis, excellent li-storage properties, and investigation of electrochemical mechanism, ACS nano. 8 (2014) 4474-4487.

[26] Y. Zhang, Y. Liu, J. Chen, Q. Guo, T. Wang, H. Pang, Cobalt vanadium oxide thin nanoplates: primary electrochemical capacitor application, Sci. Rep. 4 (2014).

[27] S. Hyun, V. Ahilan, H. Kim, S. Shanmugam, The influence of $Co_3V_2O_8$ morphology on the oxygen evolution reaction activity and stability, Electrochem. Commun. 63 (2016) 44-47.

[28] Y.-M. Hu, M.-C. Liu, Y.-X. Hu, Q.-Q. Yang, L.-B. Kong, W. Han, J.-J. Li, L. Kang, Design and synthesis of $Ni_2P/Co_3V_2O_8$ nanocomposite with enhanced electrochemical capacitive properties, Electrochim. Acta. 190 (2016) 1041-1049.

[29] W.-B. Zhang, L.-B. Kong, X.-J. Ma, Y.-C. Luo, L. Kang, synthesis and evaluation of three-dimensional $Co_3O_4/Co_3(VO_4)_2$ hybrid nanorods on nickel foam as self-supported electrodes for asymmetric supercapacitors, J. Power Sources. 269 (2014) 61-68.

[30] S. Ni, T. Li, X. Yang, Synthesis of $Co_3(OH)_2V_2O_7 \cdot 1.7H_2O$ nanosheets and its application in lithium ion batteries, Mater. Lett. 65 (2011) 2662-2664.

[31] Y. Zhao, Y. Liu, X. Du, R. Han, Y. Ding, Hexagonal assembly of $Co_3V_2O_8$ nanoparticles acting as an efficient catalyst for visible light-driven water oxidation, J. Mater. Chem A. 2 (2014) 19308-19314.

[32] M. Masjedi, N. Mir, E. Noori, T. Gholami, M. Salavati-Niasari, Effect of Schiff base ligand on the size and the optical properties of TiO_2 nanoparticles, Superlattices and Microstructures, Superlattices Microstruct. 62 (2013) 30-38.

[33] M. Masjedi-Arani, M. Salavati-Niasari, D. Ghanbari, G. Nabiyouni, A sonochemical-assisted synthesis of spherical silica nanostructures by using a new capping agent, Ceram. Int. 40 (2014) 495-499.

[34] Z. Hens, I. Moreels, B. Fritzinger, J. Martins, Ligands for Nanoparticles, J. Comprehens. Nanosci. Technol. 5 (2011) 21-49.

[35] A.K. Babaheydari, M. Salavati-Niasari, A. Khansari, Solvent-less synthesis of zinc oxide nanostructures from Zn(salen) as precursor and their optical properties, Particuology. 10 (2012) 759-764.

[36] M. Salavati-Niasari, M. Bazarganipour, characterization and catalytic oxidation properties of multi-wall carbon nanotubes with a covalently attached copper (II) salen complex, Appl. Surf. Sci. 255 (2009) 7610-7617.

[37] M. Masjedi-Arani, M. Salavati-Niasari, A simple sonochemical approach for synthesis and characterization of Zn_2SiO_4 nanostructures, Ultrason. Sonochem. 29 (2016) 226-235.

[38] M. Masjedi-Arani, M. Salavati-Niasari, Effect of carbohydrate sugars as a capping agent on the size and morphology of pure Zn_2SnO_4 nanostructures and their optical properties, Mater Lett. 174 (2016) 71-74.

[39] J. Tauc, R. Grigorovici, A. Vancu, Optical properties and electronic structure of amorphous germanium, Phys. Status Solidi B. 15 (1966) 627-637.

[40] W. Baran, A. Makowski, W. Wardas, The effect of UV radiaton absorbtion of cationic and anionic dye solutions on their photocatalytic degradation in the presence TiO_2, Dyes and Pigments. 76 (2008) 226-230.

[41] N. Laid, N. Bouanimba, R. Zouaghi, T. Sehili, Comparative study on photocatalytic decolorization of an anionic and a cationic dye using different TiO_2 photocatalysts, Desalination and Water Treatment. (2015) 1-17.

[42] K. Jeyasubramanian, G.S. Hikku, R. Krishna Sharma, Photo-catalytic degradation of methyl violet dye using zinc oxide nano particles prepared by a novel precipitation method and its anti-bacterial activities, Journal of Water Process Engineering 8 (2015) 35–44.

Figure captions:

Figure. 1. XRD patterns of cobalt vanadate nanostructures synthesized (a) at 500 ˚C (sample No.2), (b) $Co_3V_2O_8$, (c) CoV_2O_6 and (d) $Co_2V_2O_7$.

Figure. 2. SEM image of $Co_3V_2O_8$ samples with different molar ratios of Co: H_2salen (a-c) blank, (d-f) 1:0.5, (g-i) 1:1 and (j-l) 1:2.

Figure. 3. Particle size distribution of samples Nos (a-c) 3-5.

Figure. 4. SEM image of samples (a-c) CoV_2O_6 and (d-f) $Co_2V_2O_7$.

Figure. 5. TEM and HRTEM images of cobalt vanadate nanostructures (sample No.3).

Figure. 6. FT-IR spectra of samples prepared (a) $Co_3V_2O_8$, (b) CoV_2O_6 and (c) $Co_2V_2O_7$ and (d) $Co_3V_2O_8$ before calcination.

Figure. 7. EDS pattern of the samples (a) CoV_2O_6, (b) $Co_2V_2O_7$ and (c) $Co_3V_2O_8$.

Figure. 8. (a) UV–vis spectra and (b) plot of $(\alpha h\nu)^{1/2}$ versus ($h\nu$) of samples CoV_2O_6, $Co_2V_2O_7$ and $Co_3V_2O_8$.

Figure. 9. The Photocatalytic activity (a) methylene blue degradation of different cobalt vanadate nanostructures, (b) of $Co_3V_2O_8$ on degradation of different dyes (cationic and anionic), (c) of $Co_3V_2O_8$ bulk and nanostructures, (d) Influence dosage of $Co_3V_2O_8$ catalyst on the degradation percentage, (e) of $Co_3V_2O_8$ under UV and visible irradiations and (f) Chemical formula of different dyes.

Figure. 10. (a) XRD pattern and (b) FT-IR spectrum of $Co_3V_2O_8$ nanostructures after photocatalytic activity.

Scheme. 1. Schematic diagram of formation of different types of cobalt vanadate nanostructures.

Scheme 2. Schematic diagram of effect of H_2salen Schiff-base on the size, morphology and uniformity of products.

Scheme. 3. Reaction mechanism of organic dyes photodegradation over $Co_3V_2O_8$ nanostructures.

Table 1. Reaction conditions for synthesis of cobalt vanadate nanostructures.

Sample No	Product	Schiff-base ligand	Molar ratio (Co:H_2salen)	Molar ratio (Co:V)	Calcination temperature (°C)	Particle size (SEM)/nm	Average Crystallite Diameter (XRD)/nm
1	$Co_3V_2O_8$	-	-	3:2	600	Agglomerated	-
2	/$Co_2V_2O_7$ V_2O_5	H_2salen	1:0.5	3:2	500	-	-
3	$Co_3V_2O_8$	H_2salen	1:0.5	3:2	600	38.23	26.13
4	$Co_3V_2O_8$	H_2salen	1:1	3:2	600	72.91	-
5	$Co_3V_2O_8$	H_2salen	1:2	3:2	600	105.9	-
6	CoV_2O_6	H_2salen	1:0.5	1:2	600	Agglomerated	29.43
7	$Co_2V_2O_7$	H_2salen	1:0.5	1:1	600	91.80	29.64

Table. 2. The detailed crystal parameters of cobalt vanadate nanostructures

Sample	Reference code	Crystal parameters			Crystal system	Space group
		a(Å)	b(Å)	c(Å)		
$Co_3V_2O_8$	74-1486	8.3000	11.5000	6.0300	Orthorhombic	Abam
CoV_2O_6	77-1174	9.2560	3.5080	6.6260	Monoclinic	C2
CoV_2O_6	45-1052	-	-	-	Unknown	-
$Co_2V_2O_7$	70-1189	6.5940	8.3800	9.4700	Monoclinic	P21/c
$Co_2V_2O_7$	38-0193	6.5910	8.3750	9.4740	Monoclinic	P21/c
V_2O_5	41-1426	11.5160	3.5656	4.3727	Orthorhombic	Pmmn

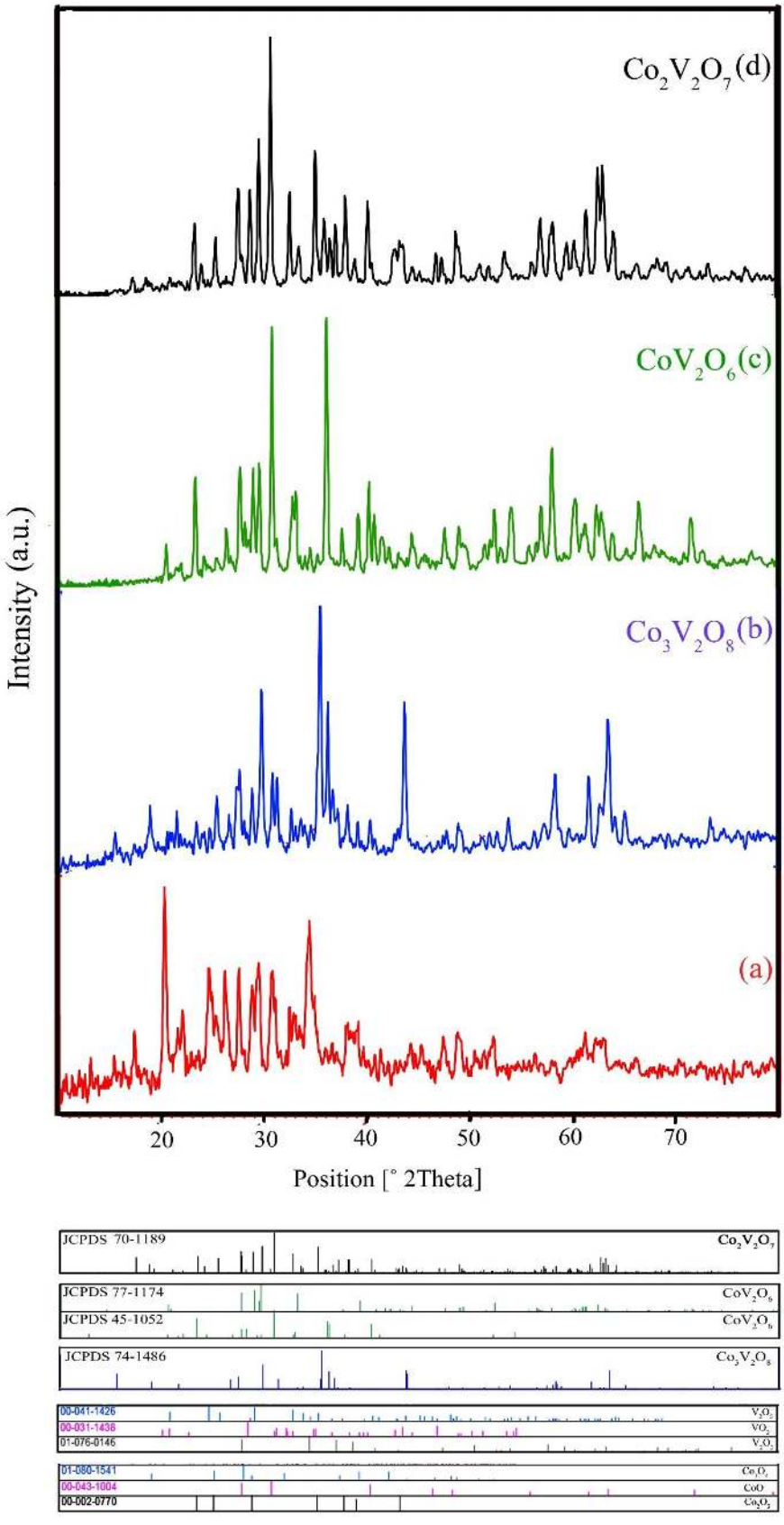
Co2V2O7(d)
CoV2O6(c)
Co3V2O8(b)
(a)
Intensity (a.u.)
20
30
40
50
60
70
Position [° 2Theta]
JCPDS 70-1189
Co2V2O7
JCPDS 77-1174
CoV2O6
JCPDS 45-1052
CoV2O6
JCPDS 74-1486
Co3V2O8
00-041-1426
00-031-1438
01-076-0146
01-080-1541
00-043-1004
CoO
00-002-0770

Figure. 1.

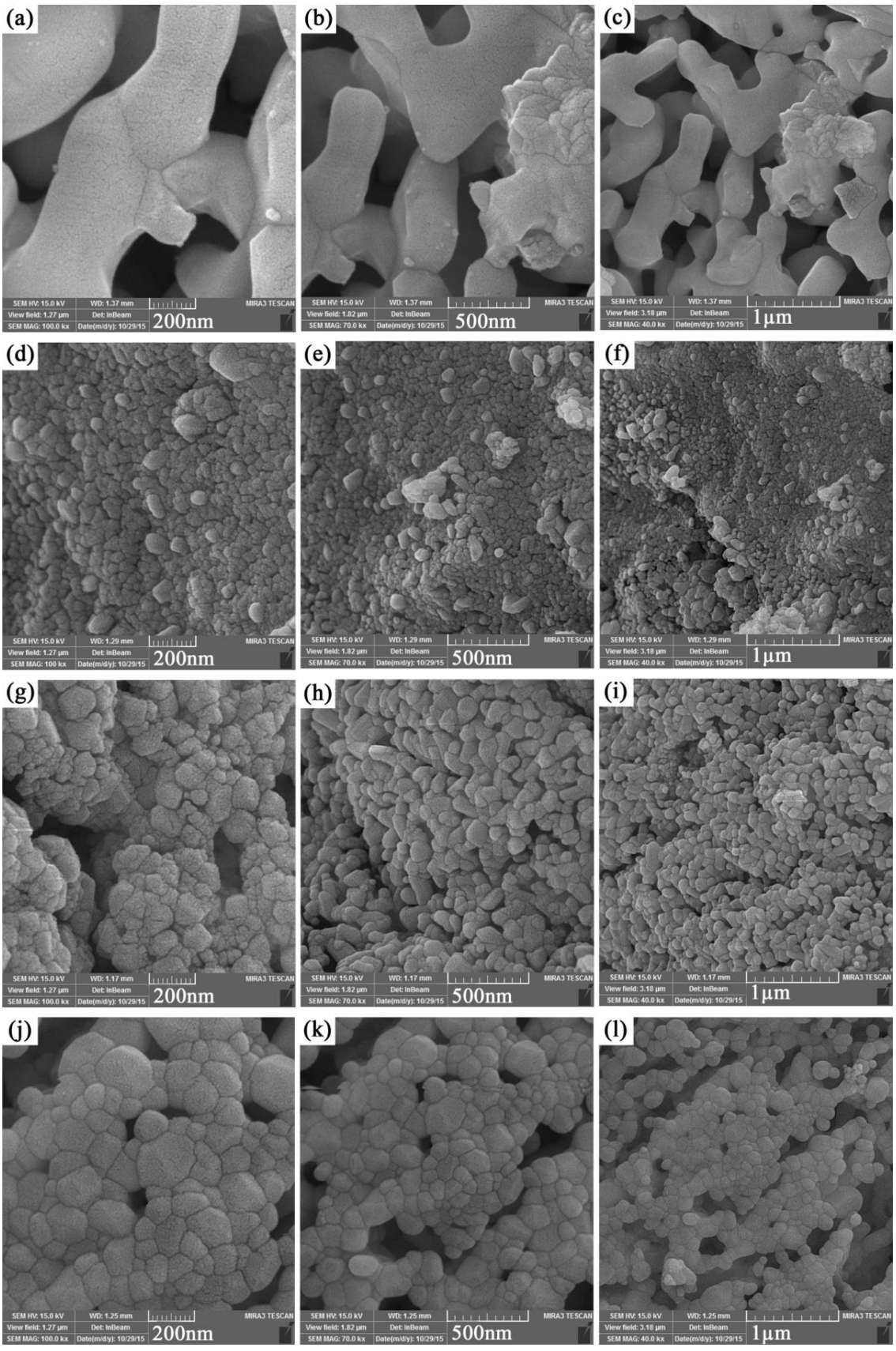

Figure. 2.

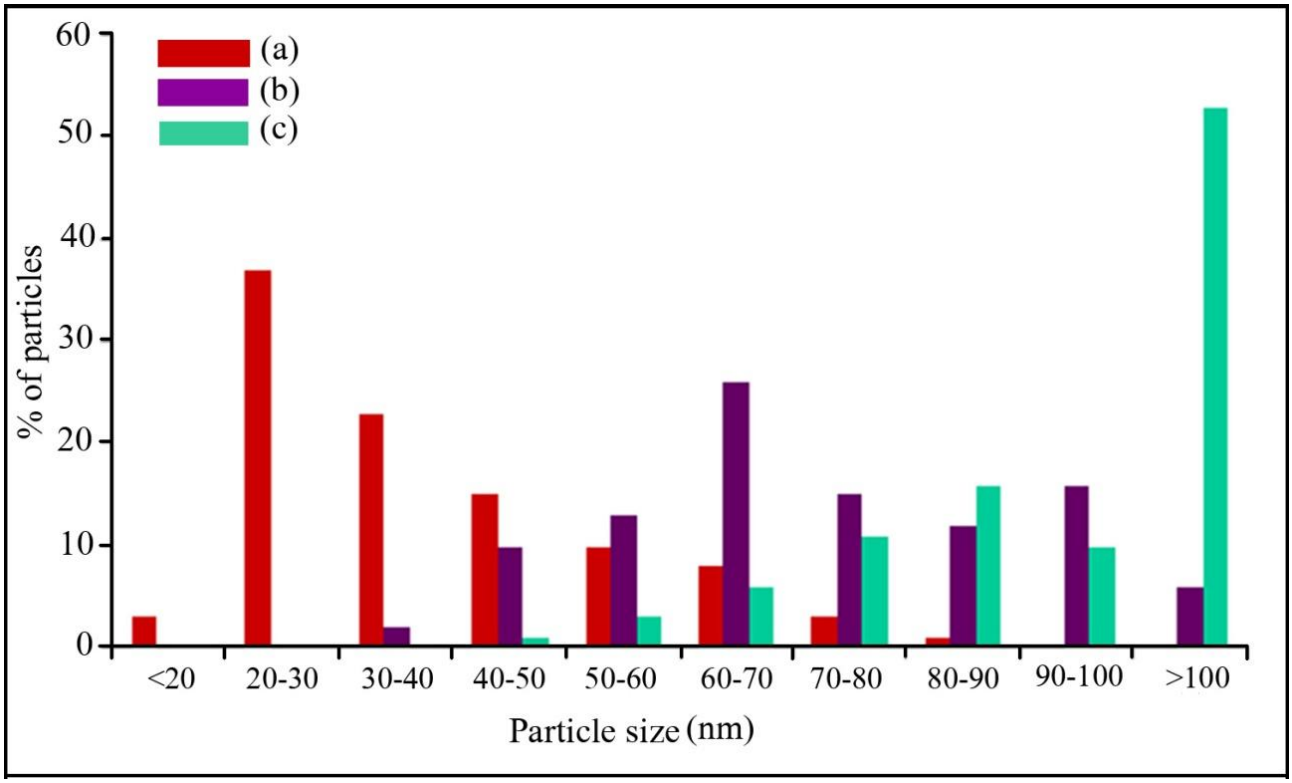
60
50
40
30
20
10
0
% of particles
(a)
(b)
(c)
<20
20-30
30-40
40-50
50-60
60-70
70-80
80-90
90-100
>100
Particle size (nm)

Figure. 3.

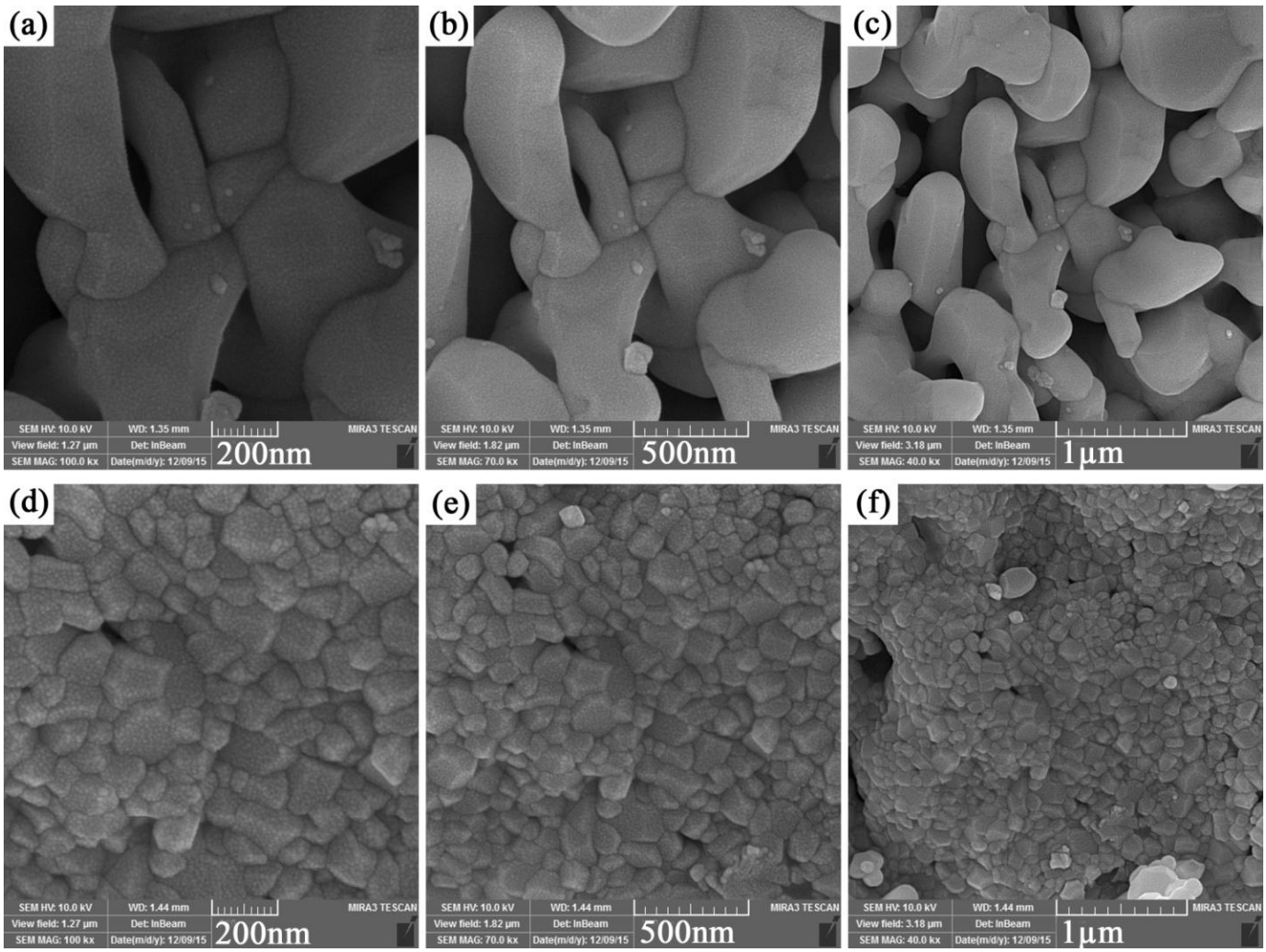
(a)
SEM HV: 10.0 kV
WD: 1.35 mm
MIRA3 TESCAN
View field: 1.27 µm
Det: InBeam
SEM MAG: 100.0 kx
Date(m/d/y): 12/09/15
200nm
(b)
SEM HV: 10.0 kV
WD: 1.35 mm
MIRA3 TESCAN
View field: 1.82 µm
Det: InBeam
SEM MAG: 70.0 kx
Date(m/d/y): 12/09/15
500nm
(c)
SEM HV: 10.0 kV
WD: 1.35 mm
MIRA3 TESCAN
View field: 3.18 µm
Det: InBeam
SEM MAG: 40.0 kx
Date(m/d/y): 12/09/15
1µm
(d)
SEM HV: 10.0 kV
WD: 1.44 mm
MIRA3 TESCAN
View field: 1.27 µm
Det: InBeam
SEM MAG: 100 kx
Date(m/d/y): 12/09/15
200nm
(e)
SEM HV: 10.0 kV
WD: 1.44 mm
MIRA3 TESCAN
View field: 1.82 µm
Det: InBeam
SEM MAG: 70.0 kx
Date(m/d/y): 12/09/15
500nm
(f)
SEM HV: 10.0 kV
WD: 1.44 mm
MIRA3 TESCAN
View field: 3.18 µm
Det: InBeam
SEM MAG: 40.0 kx
Date(m/d/y): 12/09/15
1µm

Figure. 4.

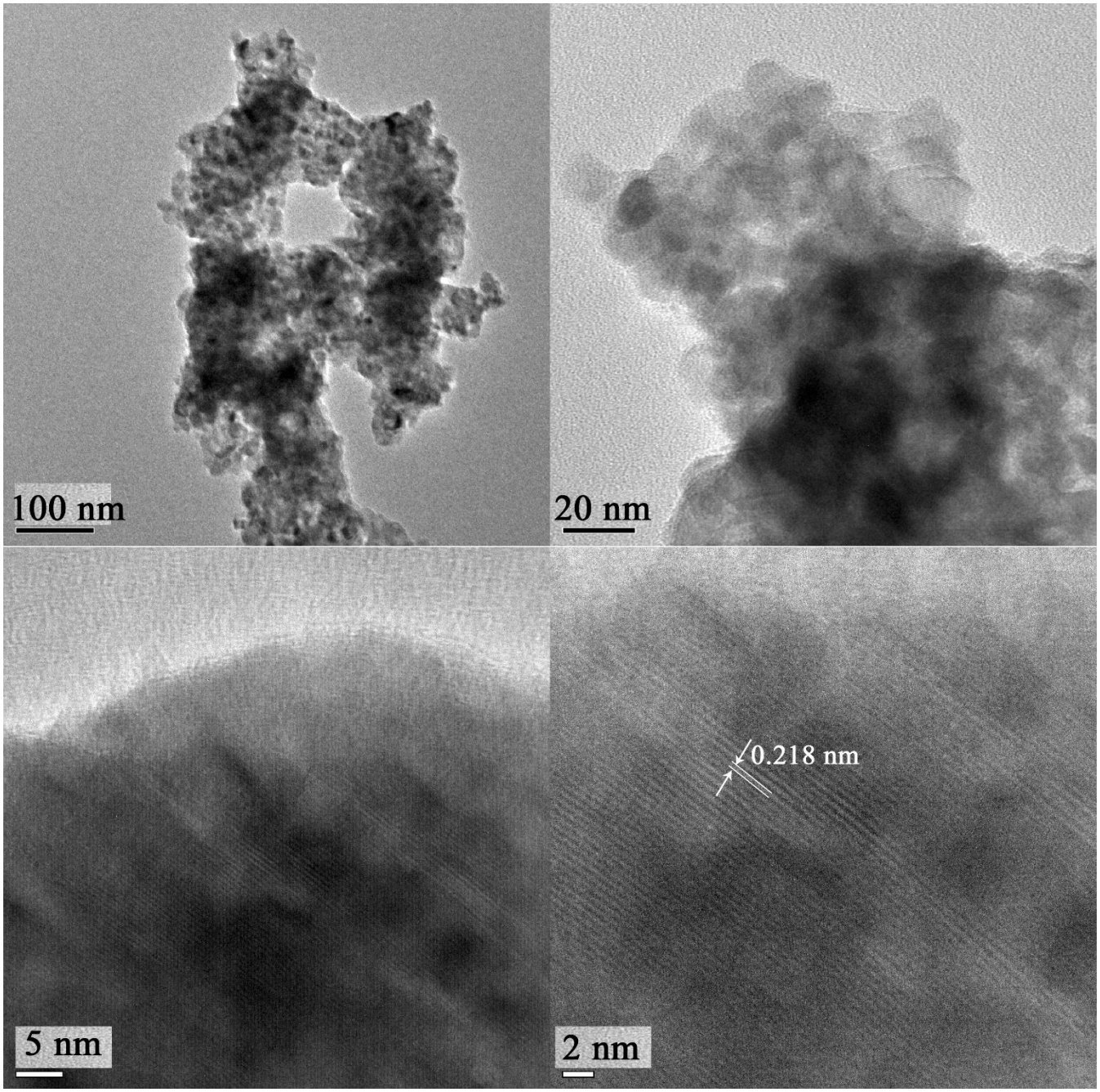

Figure. 5.

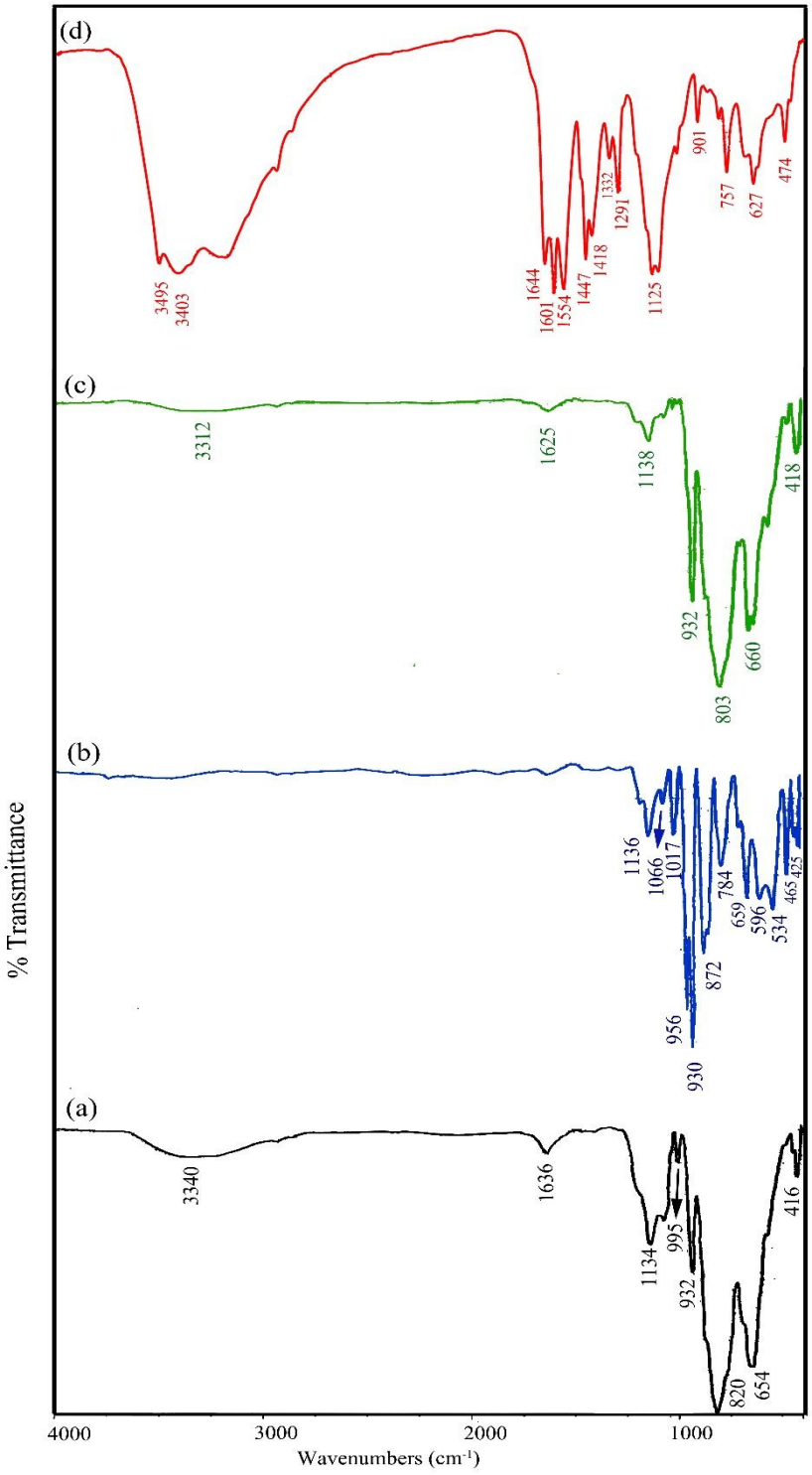
(d)
3495
3403
1644
1601
1554
1447
1418
1332
1291
1125
901
757
627
474
(c)
3312
1625
1138
932
803
660
418
(b)
1136
1066
1017
956
930
872
784
659
596
534
465
425
(a)
3340
1636
1134
995
932
820
654
416
% Transmittance
4000
3000
2000
1000
Wavenumbers (cm⁻¹)

Figure. 6.

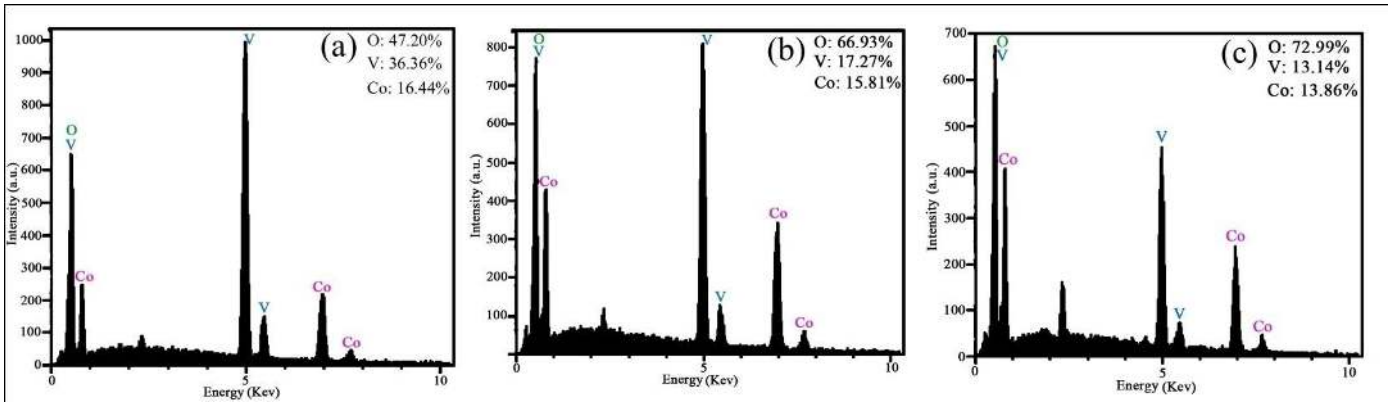
(a)
O: 47.20%
V: 36.36%
Co: 16.44%
(b)
O: 66.93%
V: 17.27%
Co: 15.81%
(c)
O: 72.99%
V: 13.14%
Co: 13.86%
Intensity (a.u.)
Energy (Kev)
O
V
Co

Figure. 7.

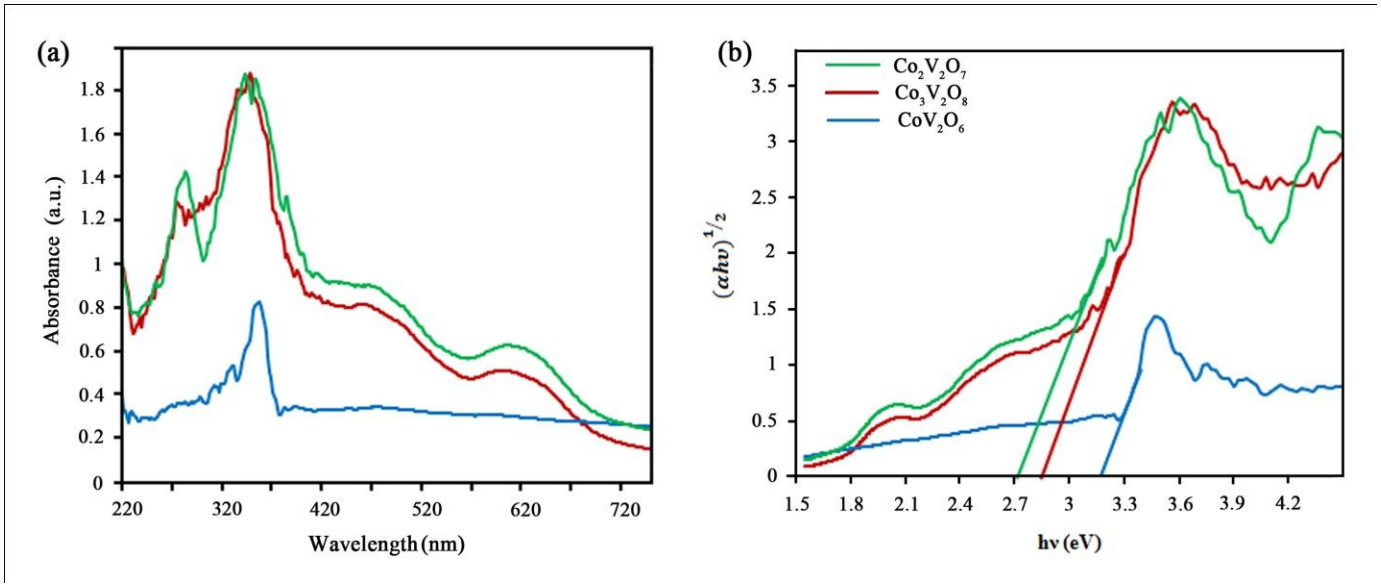
(a)
Absorbance (a.u.)
Wavelength (nm)
(b)
$Co_2V_2O_7$
$Co_3V_2O_8$
CoV_2O_6
$(\alpha h\upsilon)^{1/2}$
hv (eV)

Figure. 8.

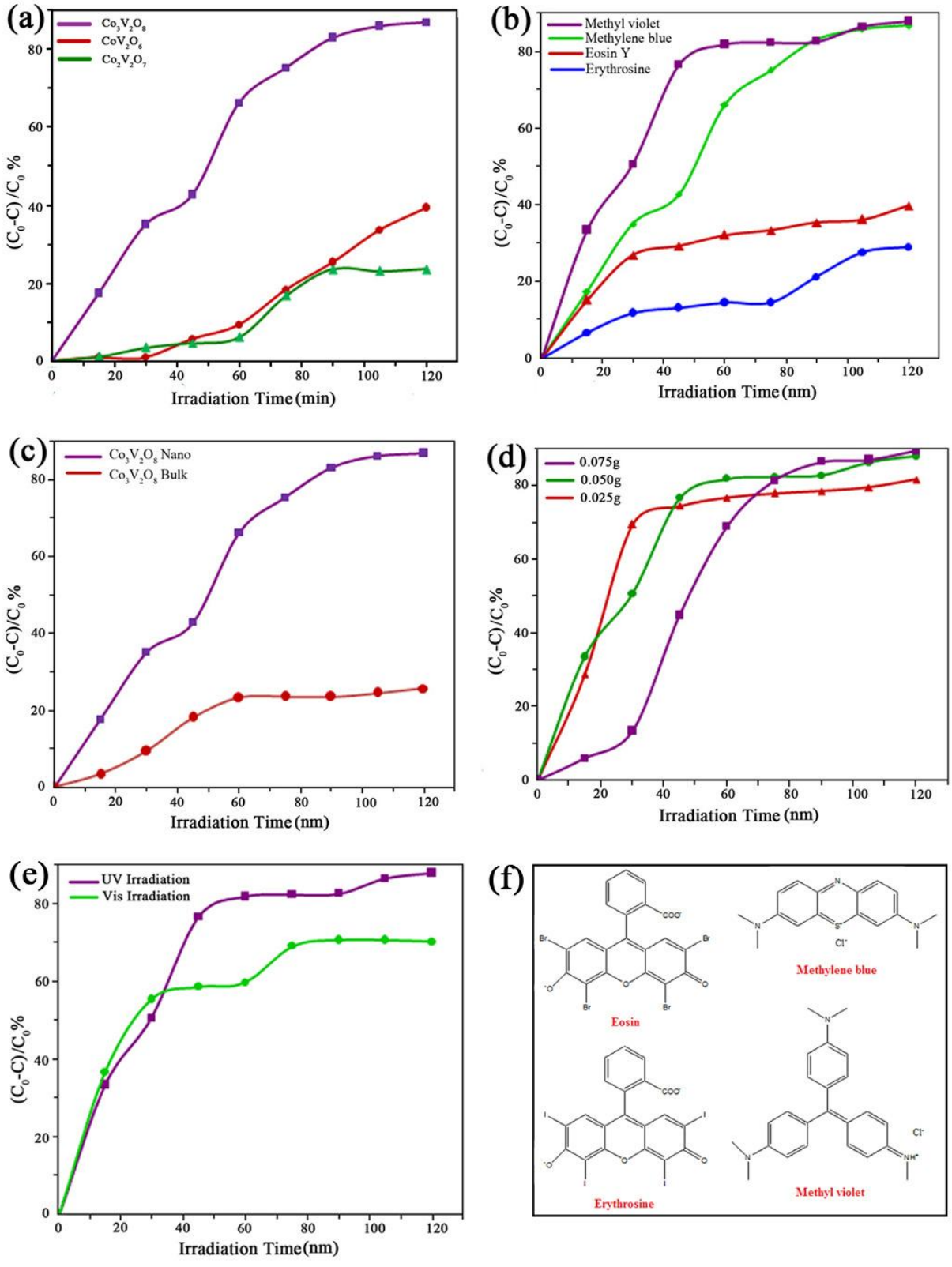
(a)
$Co_3V_2O_8$
CoV_2O_6
$Co_2V_2O_7$
$(C_0-C)/C_0$ %
Irradiation Time (min)
(b)
Methyl violet
Methylene blue
Eosin Y
Erythrosine
$(C_0-C)/C_0$ %
Irradiation Time (nm)
(c)
$Co_3V_2O_8$ Nano
$Co_3V_2O_8$ Bulk
$(C_0-C)/C_0$ %
Irradiation Time (nm)
(d)
0.075g
0.050g
0.025g
$(C_0-C)/C_0$ %
Irradiation Time (nm)
(e)
UV Irradiation
Vis Irradiation
$(C_0-C)/C_0$ %
Irradiation Time (nm)
(f)
Eosin
Methylene blue
Erythrosine
Methyl violet

Figure. 9.

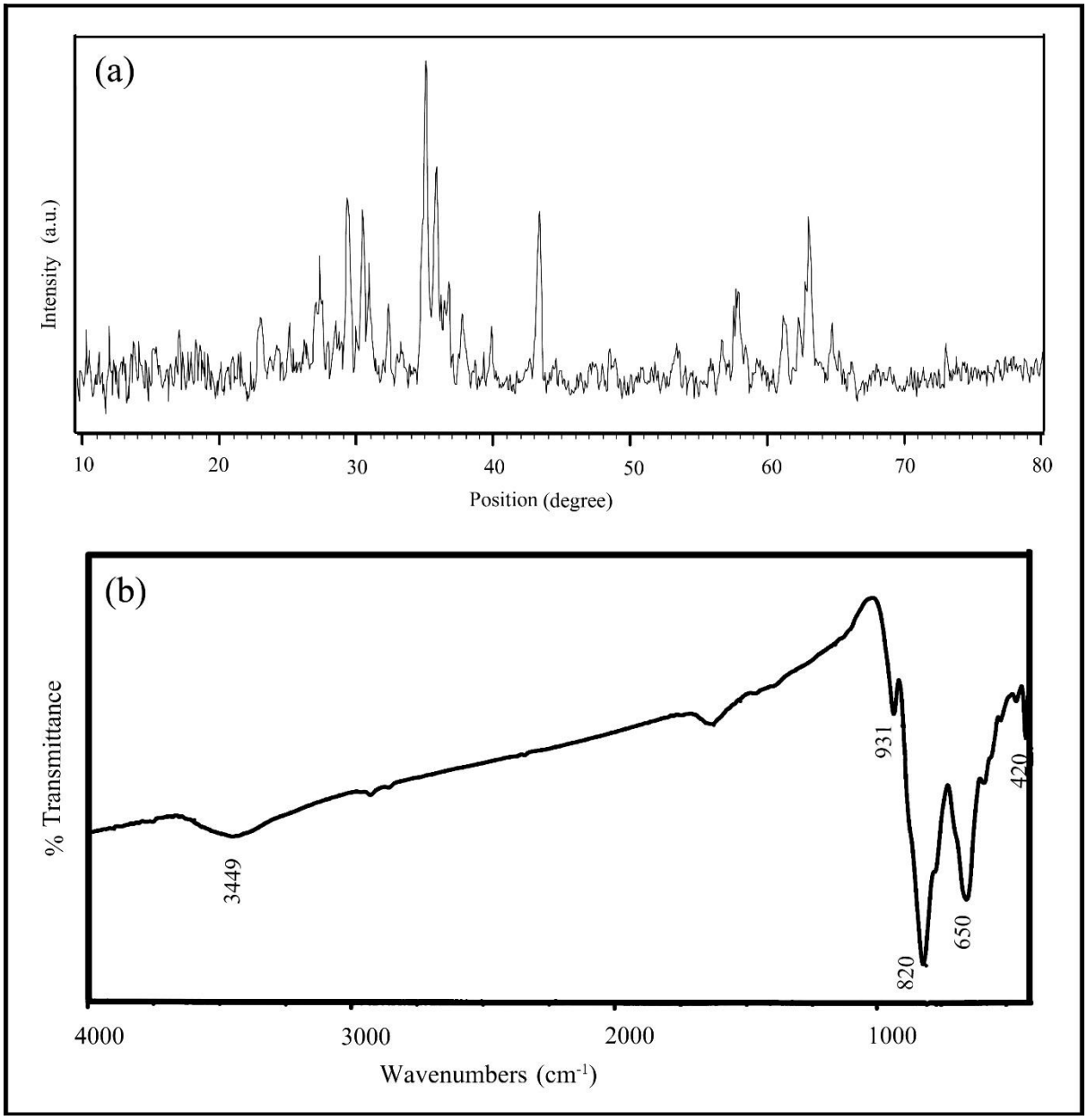

Fig. 10. (a) XRD pattern and (b) FT-IR spectrum of $Co_3V_2O_8$ nanostructures after photocatalytic activity.

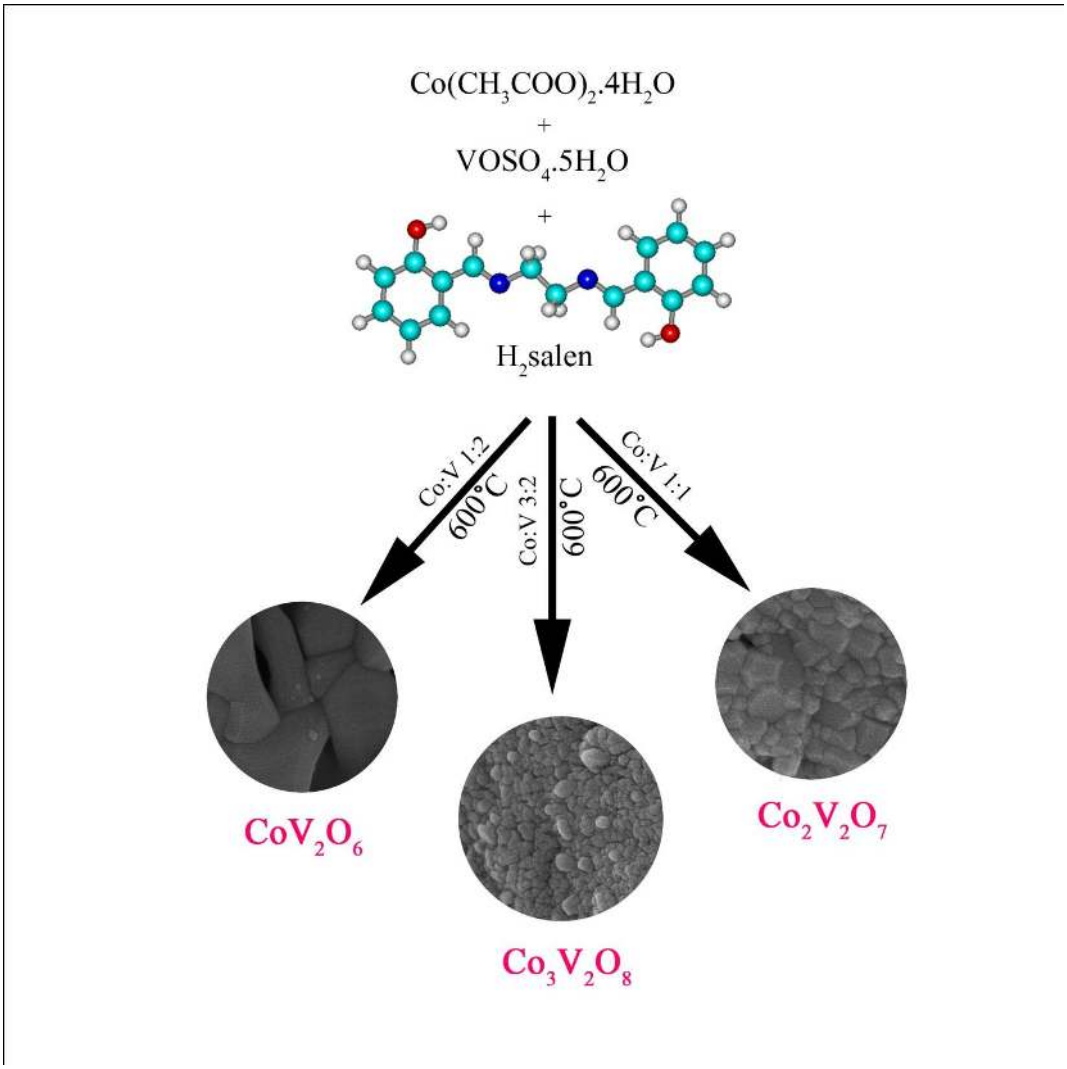

Scheme. 1. Schematic diagram of formation of different types of cobalt vnadate nanostructures

.

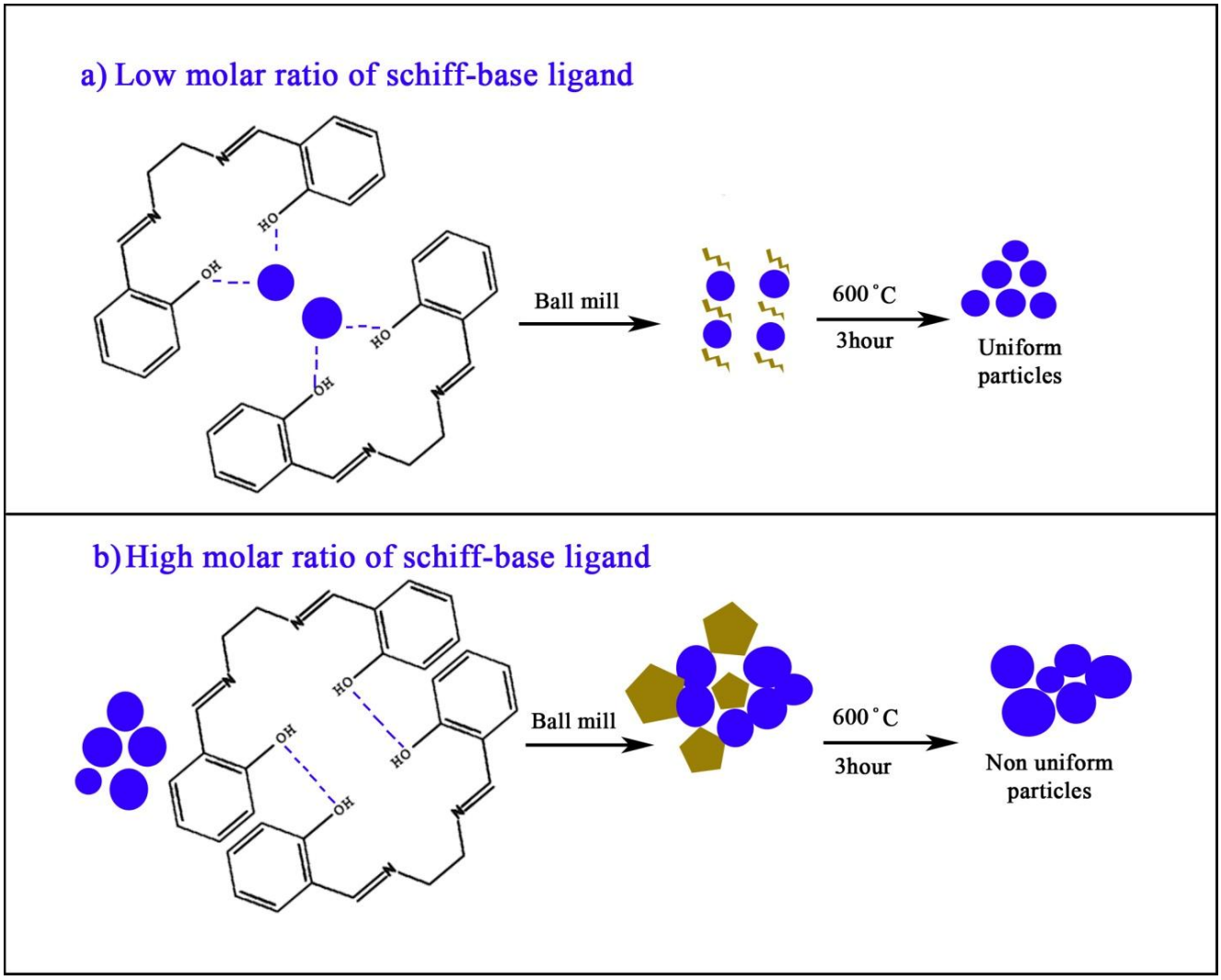
a) Low molar ratio of schiff-base ligand
Ball mill
600 °C
3hour
Uniform particles
b) High molar ratio of schiff-base ligand
Ball mill
600 °C
3hour
Non uniform particles

Scheme 2.

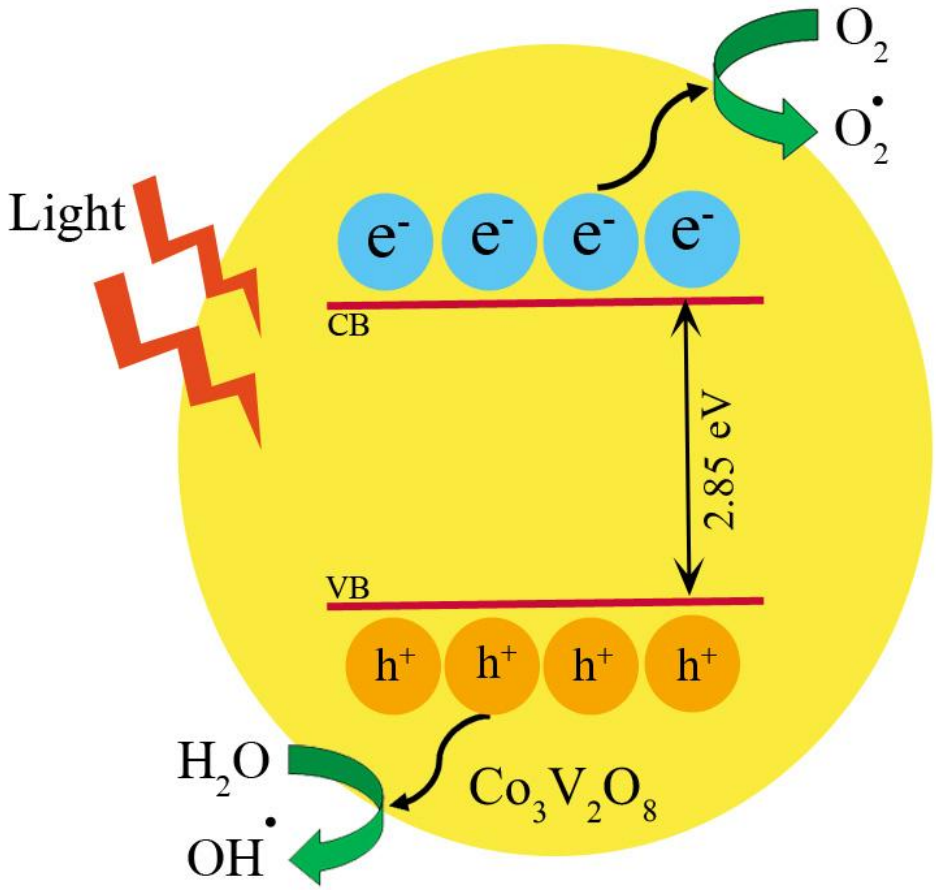

Scheme. 3.